**Supporting information for**

# Locating the precise sources of high-frequency microseisms using distributed acoustic sensing

**Han Xiao[1]*, Toshiro Tanimoto[1], Zack J. Spica[2], Beatriz Gaite[3], Sandra Ruiz-Barajas[3], Mohan Pan[4], Loïc Viens[2]**

[1]Department of Earth Science and Earth Research Institute, University of California, Santa Barbara, Santa Barbara, USA.

[2]Department of Earth and Environmental Sciences, University of Michigan, Ann Arbor, USA.

[3]National Geographic Institute of Spain, Madrid, Spain.

[4]OBS Lab, Department of Ocean Science and Engineering, Southern University of Science and Technology, Shenzhen, China.

*Corresponding author. Email: hanxiao@ucsb.edu

**This PDF file includes:**

Methods
Figures S1 to S8

## Methods

### F-K beamforming

We calculated the two-dimensional frequency-wavenumber (F-K) spectrum by applying a F-K beamforming technique to each hour of the data (Capon, 1969). The aperture of the seismic array determines the resolution of the smallest wavenumber (Schweitzer et al., 2002). Arrays with large apertures can acquire high-speed seismic waves. For ocean waves, which have relatively large wavenumbers, we used DAS data recorded over 1 kilometre (Figure S1a). To observe Scholte waves (Figure S1b), we used data recorded over 15 kilometres.

### Excitation of modes by the wave-wave interaction of wind ocean waves

The far-field Green's tensor for a spherical Earth (Dahlen & Tromp, 2021) can be written as

$$G(\mathbf{x},\mathbf{x}^{\prime};\ \omega)=\sum\frac{1}{cCI\sqrt{8\pi k_l|sin\Delta|}}\left[\hat{r}U-i\hat{k}V+i(\hat{r}\times\hat{k})W\right]\left[\widehat{r^{\prime}}\,U^{\prime}+i\widehat{k^{\prime}}\,V^{\prime}-i\left(\widehat{r^{\prime}}\times\widehat{k^{\prime}}\right)W^{\prime}\right]\times\exp\left\{-i\left(k_l\Delta+\frac{\pi}{4}\right)-\frac{\omega\Delta}{2CQ}\right\}\qquad(1)$$

where $\mathbf{x}$, $\mathbf{x}^{\prime}$, and $\omega$ are the station location, the source location, and the angular frequency ($\omega = 2\pi f$ where $f$ is the frequency), respectively. The summation is conducted for modes in each modal branch (e.g., the fundamental mode branch, the 1st overtone branch, etc.). $c$ is the phase velocity of a given mode, $C$ is the group velocity, I is the normalization for a spheroidal mode defined by $k_l = \sqrt{l(l+1)}$, $\Delta$ is the angular distance from the source to the station, $Q$ is the attenuation parameter for a given mode. Note that this equation is for the spherical Earth.

We consider a modal excitation problem by the wave-wave interaction of ocean surface waves in a flat-layered model. The horizontal displacement in the cylindrical coordinate can be defined as:

$$u_r(\omega)=\sum\frac{1}{cCI\sqrt{8\pi kr}}\left\{-iV(0)U^{\prime}(H)\right\}\times\exp\left\{-i\left(k\mathrm{r}+\frac{\pi}{4}\right)-\frac{\omega\mathrm{r}}{2CQ}\right\}\qquad(2)$$

in the radial direction (r). The normalization factor I is defined as:

$$I=\int\rho(U^2+V^2)dz\qquad(3)$$

where $U(z)$ and $V(z)$ are the vertical and horizontal eigenfunction of a spheroidal mode (Rayleigh-wave mode) and z is the vertical coordinate (positive upward) where the sea bottom is $z = 0$ and the ocean surface is $z = H$.

The wave-wave interaction of ocean waves near the ocean surface generates pressure (Longuet-Higgins, 1950) and with an introduction of a surface area $dS$, it creates a vertical force $f = -pdS$. This force can be multiplied to the above formula to obtain the generation of horizontal displacements at sea floor.

Since DAS measures strain along the fibre-optic cable, we differentiate the above formula with respect to $\boldsymbol{r}$ and derive the following formula for the extensional strain in the radial direction:

$$e_{rr}(\omega) = \sum \frac{1}{cCI}\sqrt{\frac{k}{8\pi r}}\{-V(0)U^{'}(H)\} \times \exp\{-i\left(kr + \frac{\pi}{4}\right) - \frac{\omega r}{2CQ}\} \tag{4}$$

where we only kept the term that differentiates the exponential oscillation term. Differentiation with respect to $1/\sqrt{r}$ should rapidly become small with distance and the differentiation of the attenuation term should also be small. In this formula, $k$ is the horizontal wavenumber. We can rewrite this formula as

$$e_{rr}(\omega) = \sum a_s \exp\{-i\left(kr + \frac{\pi}{4}\right) - \frac{\omega r}{2CQ}\} \tag{5}$$

where $a_s$ is the excitation coefficient for a mode defined by:

$$a_s = \frac{1}{cCI}\sqrt{\frac{k}{8\pi r}}\{-V(0)U^{'}(H)\} \tag{6}$$

The efficiency of excitation of various mode branches is related to the size of this term and is computed for various models.

**Modal analysis**

We vary the ocean depth from 25 m to 500 m and examine the effects on modal excitations. Below the sea bottom, all models have a sedimentary layer of a thickness of 1 km (density ($\rho$): 2000 kg/m$^3$, Vp: 2.0 km/s, Vs: 1.0 km/s), a transition layer with a thickness of 1 km where $\rho$ and seismic velocities increase linearly with depth and finally connect to the parameters from the PREM model (1981). The PREM parameters are assumed from 2 km below the sea bottom. PREM has the upper crustal parameters of $\rho$: 2600 (kg/m$^3$), Vp: 2.6 (km/s), Vs: 3.2 (km/s), and the parameters after transition to lower crust are $\rho$: 2900 (kg/m$^3$), Vp: 6.8 (km/s), Vs: 3.9 (km/s).

In Figure S2, we show an example of the modal analysis performed with a model that has an ocean depth of 100 m. We use a code for spherical modes that incorporates gravity effects. Therefore, for each wavenumber (horizontal wavelength), we first obtain a tsunami mode with a phase velocity of $\sqrt{gH}$. Figure S2 shows overtone modes up to the 4$^{th}$ one. The fundamental mode is termed as the Scholte mode for the reasons listed below.

Figure S3 shows the same set of modes. Tsunami modes are confined to the low-frequency range (e.g., below 0.2 Hz) and do not appear in the 0.5-2.0 Hz frequency range, which is the focus of this work. The phase velocity of Scholte waves for frequencies above 0.5 Hz (e.g., 0.8-1.0 km/s) shows good agreement with Figure S1b. It supports that we mainly observe the effects of Scholte waves. Eigenfunctions of four modes at 1 Hz, indicated by solid circles in Figure S3, are shown in Figure S4.

We name the fundamental mode as the Scholte mode in this paper because eigenfunctions have their maximum amplitudes at the seabed (Figure S4). The amplitudes tend to decay up and down from the seafloor, although strictly speaking, they deviate from what were originally known as Scholte waves, which were trapped at the fluid-solid interface on the seafloor.

The excitation coefficients of these modes are shown in Figure S5. This figure shows clearly that the wave-wave interactions at the ocean surface preferentially excite Scholte modes. The effect of the ocean depth on the excitation coefficients is shown in Figure S6. This figure shows that the results in Figure S5 remain very similar from 25 m to 100 m in depth, which are relevant to this study. It also shows that ocean depths deeper than 200 m show much less excitation of Scholte modes. This suggests that the excitation efficiency may greatly differ if the ocean depth steeply increases near the coast.

## References


Capon, J. (1969). High-resolution frequency-wavenumber spectrum analysis. *Proceedings of the IEEE, 57*(8), 1408-1418.

Dahlen, F. A., & Tromp, J. (2021). Princeton University Press. https://doi.org/10.1515/9780691216157

Longuet-Higgins, M. S. (1950). A Theory of the Origin of Microseisms. *Philosophical Transactions of the Royal Society of London A-Mathematical and Physical Sciences, 243*(857), 1-35. https://doi.org/10.1098/rsta.1950.0012

Schweitzer, J., Fyen, J., Mykkeltveit, S., Kværna, T., & Bormann, P. (2002). Seismic arrays. *IASPEI new manual of seismological observatory practice*, 1-51.

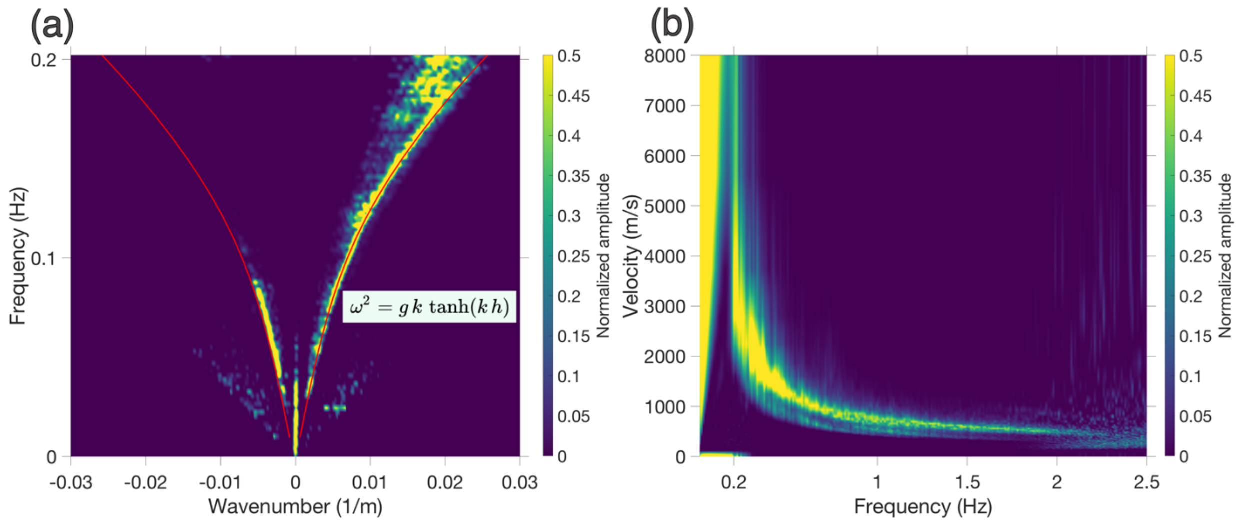


**Figure S1.** One-hour F-K beamforming analysis for DAS data on September 3rd, 2020. (a) The data are taken between 8 and 9 km from the coast, where the water depth is about 40 m. The red lines represent the theoretical dispersion curve of ocean surface gravity waves for a water depth of 40 m. (b) The phase velocity of Scholte waves was observed between 25 and 40 km from the coast versus frequency. Clear surface-wave dispersion can be seen for frequencies higher than 0.2 Hz. Note that our analysis focuses on the 0.5-2.0 Hz frequency range.

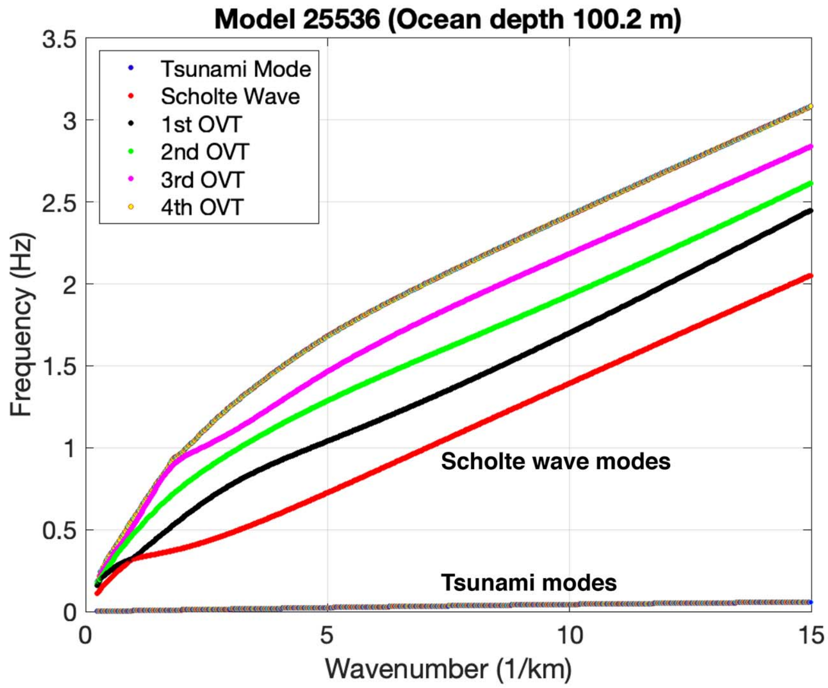


**Figure S2.** Eigenfrequencies plotted against wavenumber. For each horizontal wavenumber, the lowest mode is the tsunami mode (equivalent mode). The fundamental mode is named as Scholte wave or Scholte mode because of a large horizontal motion peak at the sea bottom. The first four modes (overtones: OVT) are shown in this plot.

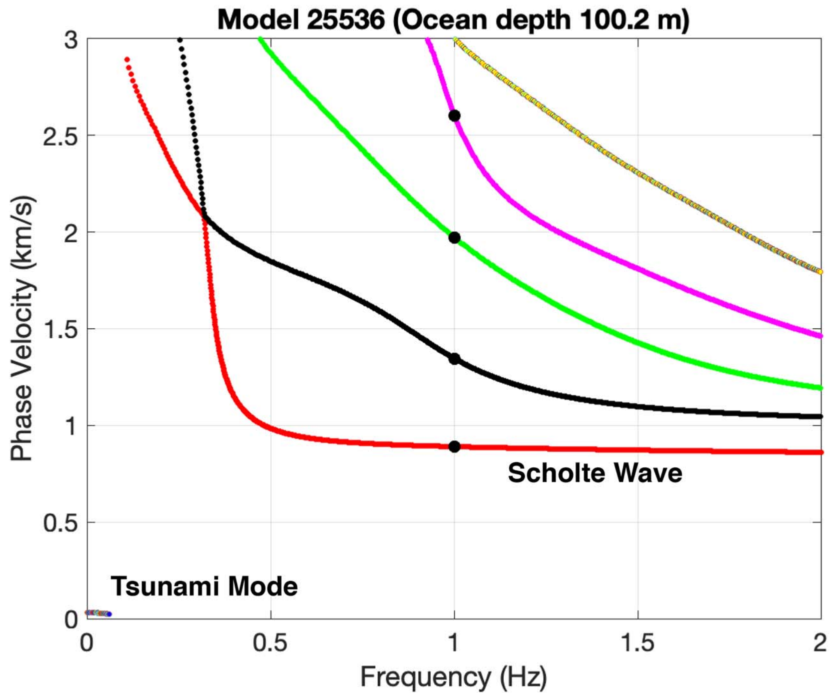


**Figure S3.** Phase velocity of the normal modes plotted against frequency. Color code is the same as in Figure S2.

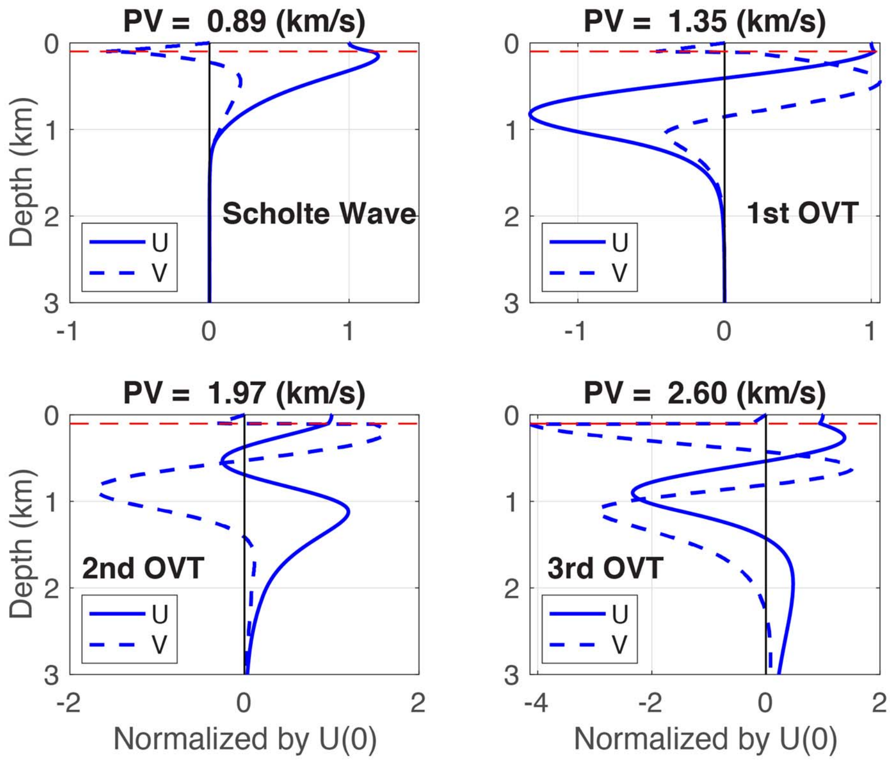


**Figure S4.** Eigenfunctions of four modes at 1 Hz, indicated by solid circles in Figure S3. The eigenfunctions of the Scholte waves (upper left) are very similar to that of Rayleigh waves on land, except for the behaviors in the ocean. The red dashed line is sea bottom.

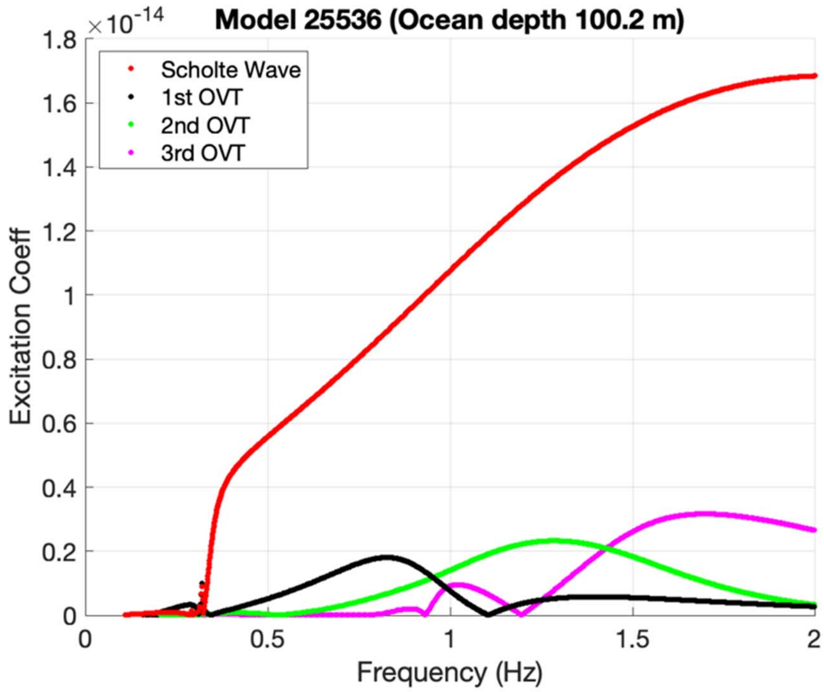


**Figure S5.** Excitation coefficients $|a_s|$ of Scholte modes. The fundamental mode (the red dots), $1^{st}$ (the black dots), $2^{nd}$ (the green dots), and $3^{rd}$ (the purple dots) overtones (OVT) of Scholte waves are shown. For horizontal strain at the ocean bottom, the contributions from Scholte waves are dominant.

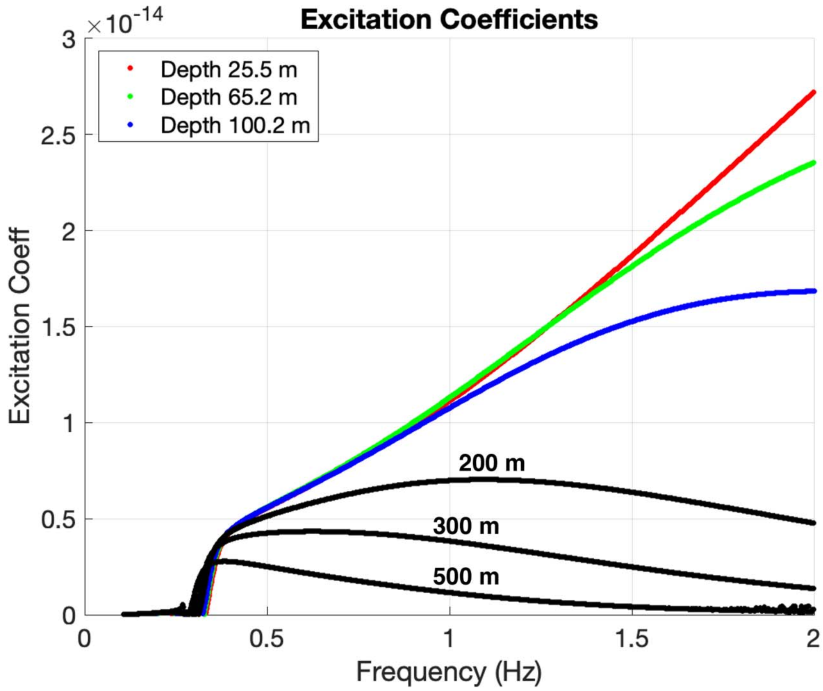


**Figure S6.** Excitation coefficients at different depths. We observe the excitation sources changing in the area where ocean depth varies from 25 m to 100 m. Three cases within this depth range are shown in color and agree between 0.5 Hz and 1.0 Hz. Three cases for the deeper ocean, 200 m, 300 m, and 500 m, show that the excitation efficiency by the wave-wave interaction of ocean surface waves decreases quickly with depth.

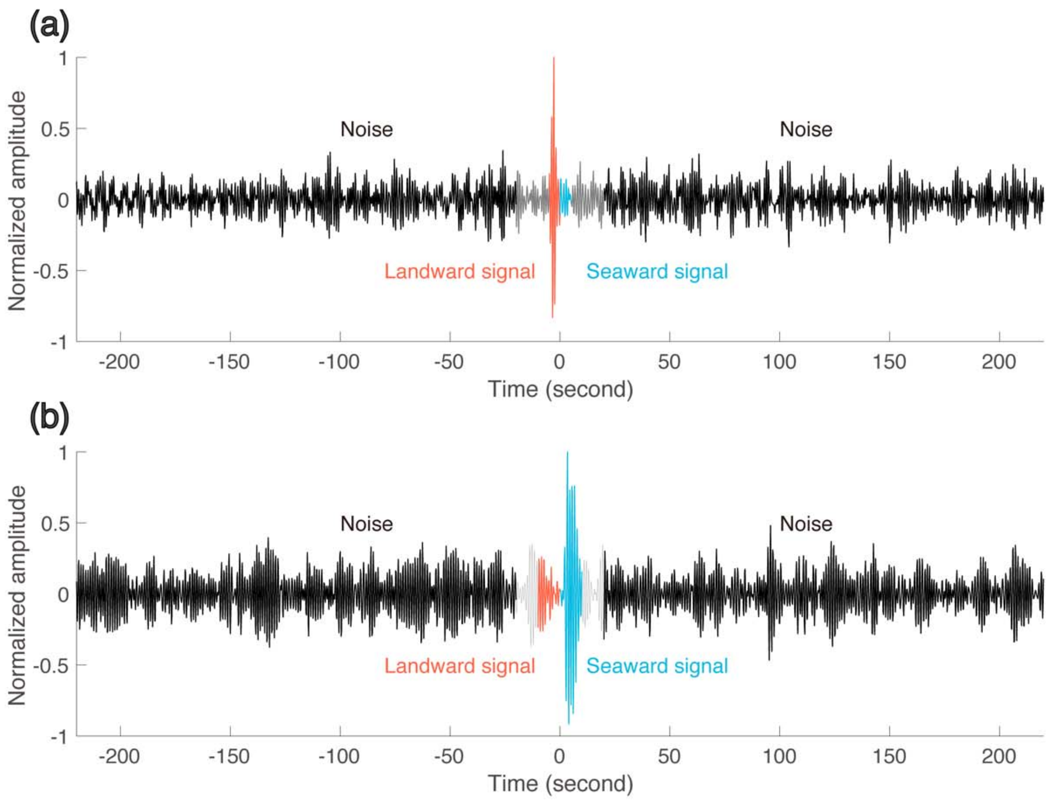


**Figure S7.** Examples of Cross-Correlation Functions. (a) CCF between channels 300-305 (channel 300 is at 5.0 km from the coast) and channels 390-395 (channel 390 is at 6.5 km from the coast) in the frequency band 0.5-1 Hz. The red and blue lines show the Scholte wave selected in this study. The causal (blue) and acausal (red) parts relates to the seaward and landward propagations of Scholte waves. The black line shows the trailing coda for a duration of 200 sec. We calculated the signal-to-noise ratio (SNR) by using the maximum amplitude of the signals (red and blue) divided by the mean value of 200 seconds of trailing coda (black). (b) Same as (a) for channels 2000-2005 (channel 2000 is at 33.6 km from the coast) and channels 2090-2095 (channel 2090 is at 35.1 km from the coast).

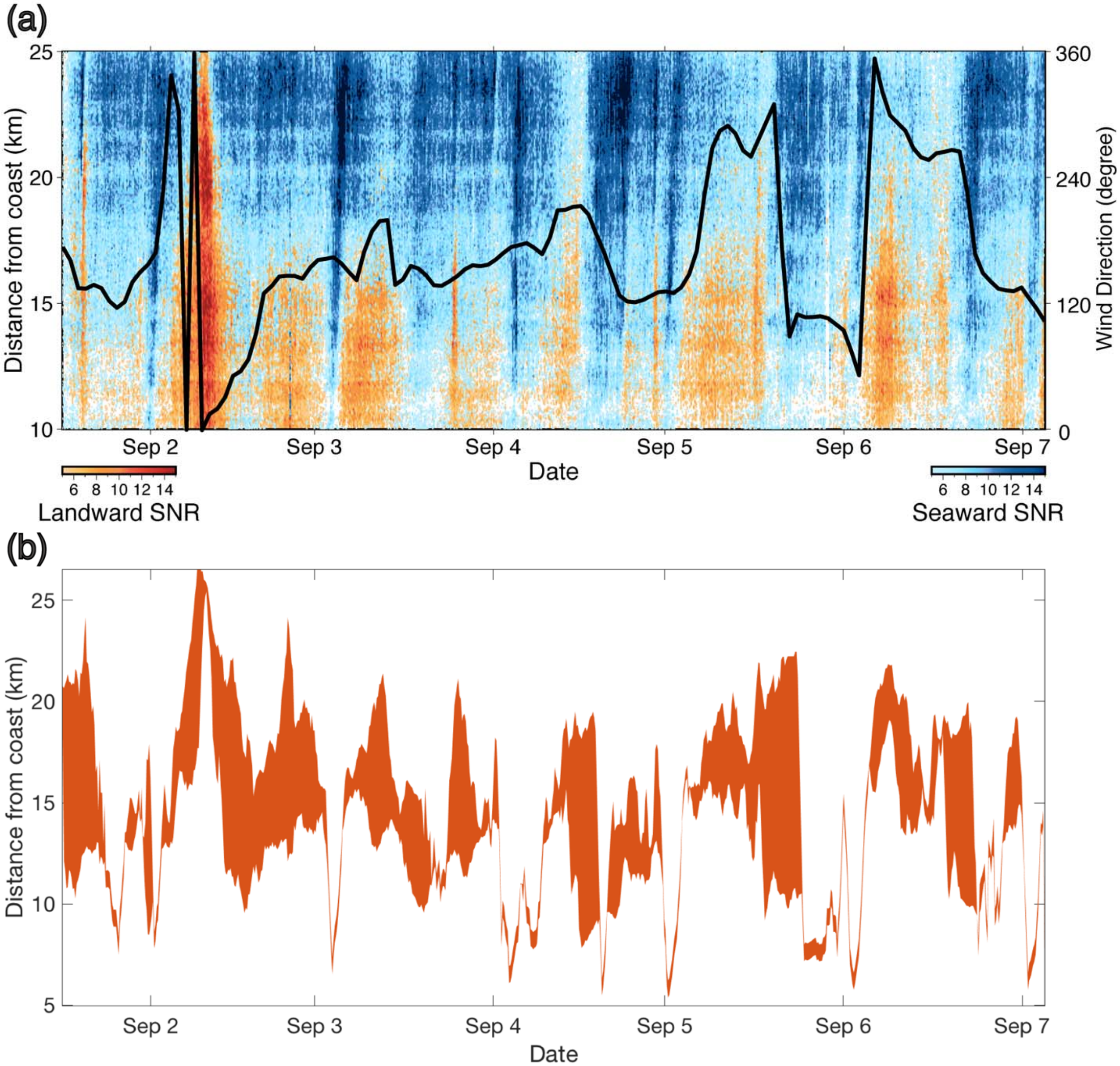


**Figure S8.** HF microseisms source locations in the frequency band 1-2 Hz. (a) The SNR of the Scholte waves in the frequency band 1-2 Hz as a function of time for the seaward (blue) and landward direction (red) propagation. The position between the two-color series represents the source location of the HF microseism. The black line represents the local wind direction change recorded at the location marked in Figure 1a. (b) The source regions of HF microseisms in the frequency band 1-2 Hz. We define the source locations of the HF microseisms as the SNR of both seaward and landward propagating Scholte waves larger than 5.

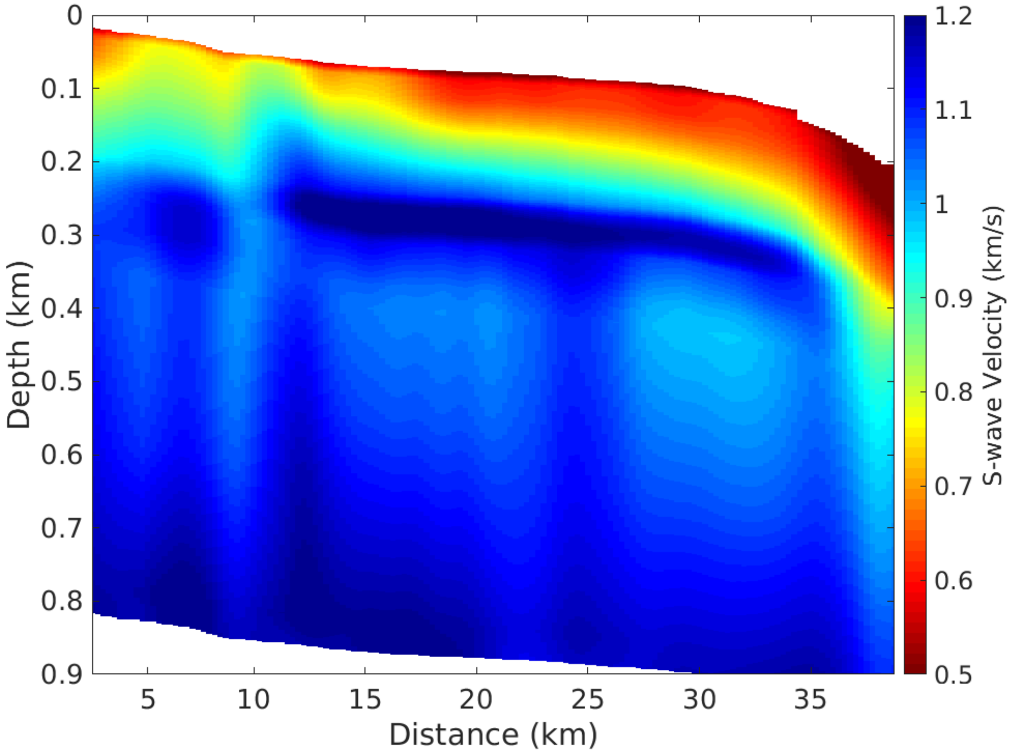


**Figure S9.** Shear-wave velocity profile obtained from ambient noise cross-correlation functions. Each dispersion curve is calculated at each subset of 4 km.